Facile Synthesis of Monodispersed Mesoporous Silica Nanoparticles with Ultralarge Pores and Their Application in Gene Delivery

Mi-Hee Kim,[†] Hee-Kyung Na,[†] Young-Kwan Kim,[†] Soo-Ryoon Ryoo,[†] Hae Sung Cho,[†] Kyung Eun Lee,[‡] Hyesung Jeon,[‡] Ryong Ryoo,[†,§] and Dal-Hee Min[†,*]

[†]Department of Chemistry and [§]Graduate School of Nanoscience and Technology (WCU), KAIST, Daejeon 305-701, Korea, and [‡]Biomedical Research Center, Korea Institute of Science and Technology, Seongbuk-gu, Seoul 136-791, Korea

ABSTRACT Among various nanoparticles, the silica nanoparticle (SiNP) is an attractive candidate as a gene delivery carrier due to advantages such as availability in porous forms for encapsulation of drugs and genes, large surface area to load biomacromolecules, biocompatibility, storage stability, and easy preparation in large quantity with low cost. Here, we report on a facile synthesis of monodispersed mesoporous silica nanoparticles (MMSN) possessing very large pores (>15 nm) and application of the nanoparticles to plasmid DNA delivery to human cells. The aminated MMSN with large pores provided a higher loading capacity for plasmids than those with small pores (~2 nm), and the complex of MMSN with plasmid DNA readily entered into cells without supplementary polymers such as cationic dendrimers. Furthermore, MMSN with large pores could efficiently protect plasmids from nuclease-mediated degradation and showed much higher transfection efficiency of the plasmids encoding luciferase and green fluorescent protein (pLuc, pGFP) compared to MMSN with small pores (~2 nm).

KEYWORDS: biocompatibility · gene delivery · large pores · plasmid · porous silica nanoparticle

Gene therapy has been considered an important therapeutic option for the treatment of genetically caused diseases such as cancer,[1−3] hepatitis,[4,5] and sickle-cell anemia.[6,7] Such therapy necessitates efficient gene delivery to cells because naked nucleic acids alone are not able to get across cell membranes. Gene delivery systems are divided into two methods—viral and nonviral systems. Viral systems, which harness the infection mechanism of natural viruses, are evidently most effective but possess safety issues such as immunogenicity and the possibility of gene recombination.[8] Nonviral gene delivery methods based on chemical methods involve cationic compounds,[9] recombinant proteins,[10] or polymeric[11] or inorganic nanoparticles.[12] Cationic compounds usually exhibit high toxicity, and recombinant proteins require a high cost to prepare. The major drawback of polymeric systems involving poly(L-lysine) (PLL) and polyethylenimine (PEI) is high toxicity.[13]

Inorganic nanoparticles possess several advantages over polymeric ones for gene delivery system.[14] With the advancement of nanotechnology, many inorganic nanoparticles could be easily prepared, and surface modification becomes straightforward. Some of inorganic nanoparticles have relatively low toxicity and can be engineered to have less cytotoxicity. Most of them can be stored with high long-term stability. To date, many different kinds of inorganic nanoparticles have been used for gene delivery, such as gold,[15,16] quantum dot,[17,18] calcium phosphate,[19] carbon nanotubes,[20,21] and silica.[22] Deoxyribonucleic acids (DNAs) that are conjugated or adsorbed onto a nanoparticle surface can be easily degraded by nucleases. Therefore, DNAs are preferred to be packaged into a suitable space for protection from degradation until they arrive where they should be released inside cells. Among various nanoparticles, the silica nanoparticle (SiNP) is attractive because it has such advantages as availability in porous forms, easy surface manipulation, biocompatibility, long-term stability, and ease of preparation in large quantity with low cost. In fact, porous SiNPs with small pore size (~2.7 nm) have been utilized for plasmid delivery. Xia, T. *et al*. reported the use of SiNPs modified with PEI to adsorb negatively charged plasmid DNA onto the surface for loading and cellular delivery.[23] Others used cationic materials such as dendrimer[24] and cationic lipid[25] for surface modification. Modification of the surface with cationic components was necessary

* Address correspondence to dalheemin@kaist.ac.kr.

Received for review November 18, 2010 and accepted March 31, 2011.

Published online March 31, 2011
10.1021/nn103130q

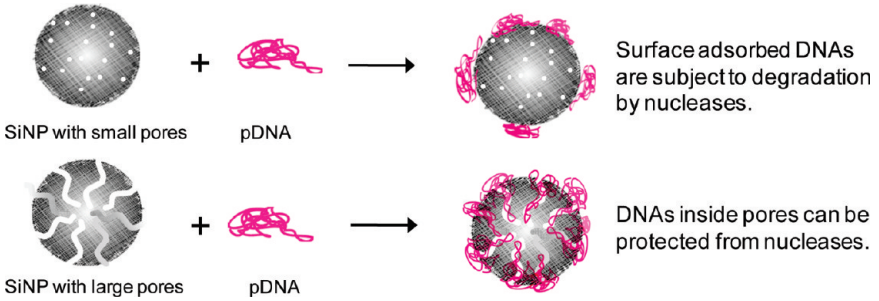

Scheme 1. Monodispersed mesoporous silica nanoparticles (MMSN) with large pores are expected to give higher loading capacity for plasmid DNA (pDNA) compared to those with small pores and better protection from nucleases.

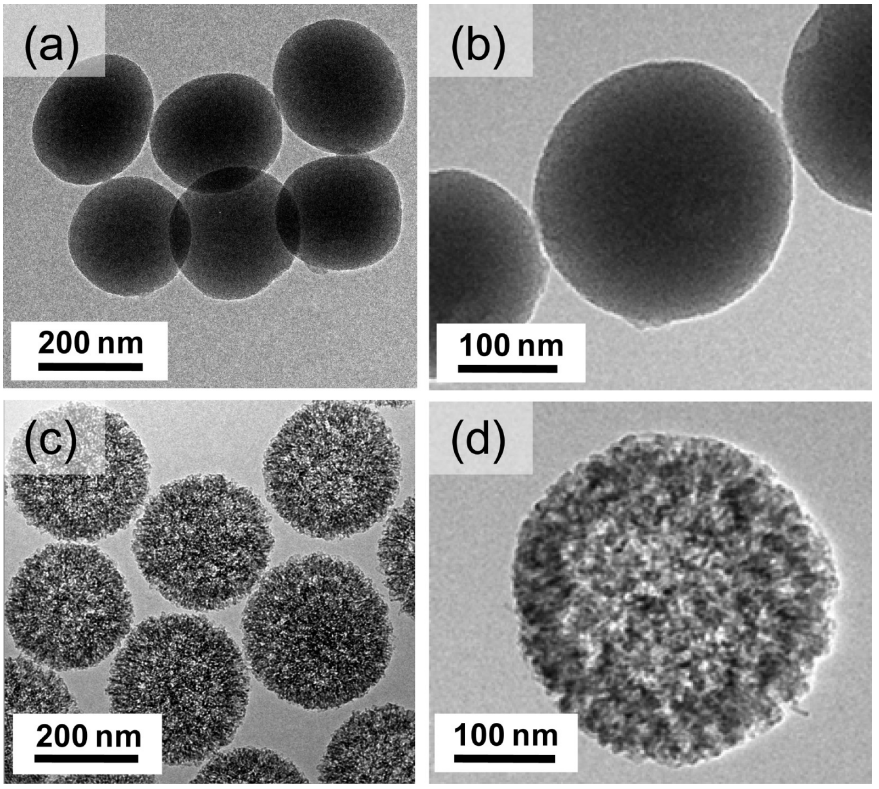

Figure 1. TEM images of (a, b) nonexpanded monodispersed mesoporous silica nanoparticles (MMSN-2) and (c, d) expanded monodispersed mesoporous silica nanoparticles (MMSN-23).

for DNA adsorption.[26−28] In these strategies, plasmids cannot be effectively protected from nucleases and cationic coating materials can increase cytotoxicity of the whole gene carrier. Therefore, porous SiNP with very large pores should be useful to accommodate large plasmid DNAs by providing more inner space to hold DNA for better protection against nucleases.

Here, we report on a facile synthesis of monodispersed mesoporous silica nanoparticles (MMSN) possessing very large pores (>15 nm) and application of the nanoparticle to plasmid DNA delivery to human cells. The aminated MMSN with large pores provide cationic pores large enough to encapsulate plasmids, at least partially, without supplementary polymers such as PEI (Scheme 1).

RESULTS AND DISCUSSION

Preparation of MMSN with Large Pores. We prepared MMSN possessing large pores (>15 nm in diameter) according to a swelling agent incorporation method[29] with a slight modification. 1,3,5-Trimethylbenzene (TMB) was used for swelling of the mesopores with a mixed solvent of water and ethanol. Mesopores were expanded to about 10 times the size (23 nm, mean pore size) of the original one (2.1 nm)[30] when equal volumes of TMB, water, and ethanol were used, according to nitrogen sorption data. Transmission electron microscopy (TEM) images indicate that the prepared MMSN had outer diameter of about 250 nm, while retaining high monodispersity and spherical morphology (Figure 1). To endow the positively charged surface

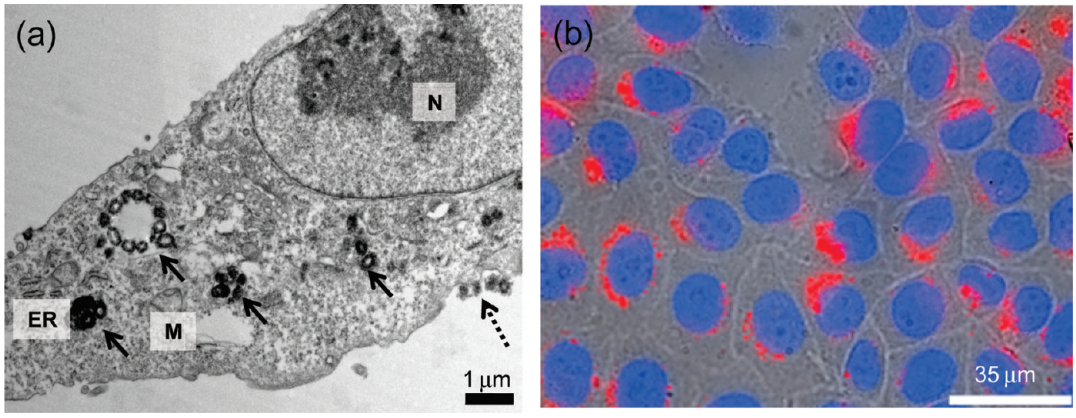

Figure 2. TEM (a) and fluorescence (b) images of HeLa cells with internalized MMSN-23. Black solid and dotted arrows in the TEM image indicate MMSN-23 that underwent cellular uptake and that are about to enter into cells, respectively. Red fluorescence represents location of MMSN-23 inside cells, arising from TAMRA dyes that are conjugated to MMSN-23. Nuclei are stained with DAPI, showing blue fluorescence (b). The cell images confirmed that MMSN-23 readily enter into cells across cell membranes without further surface treatment and without cationic polymers or lipids.

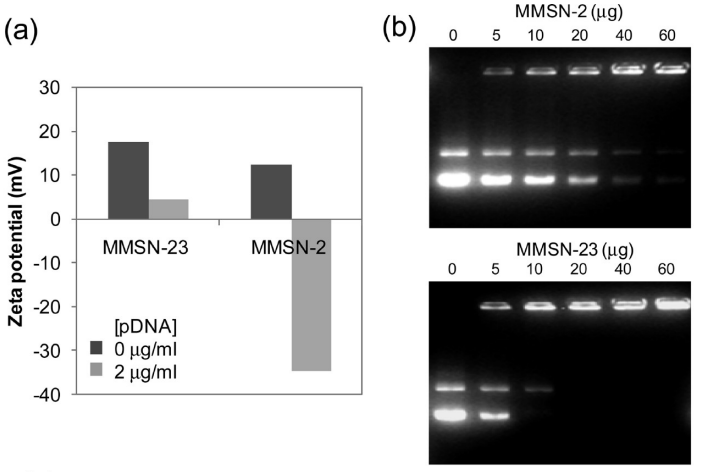

(c)

Amount of used MMSN	number of pDNA per MMSN-2	number of pDNA per MMSN-23
20 μg	15.0	36.6
40 μg	11.4	18.3
60 μg	8.8	12.2

Figure 3. (a) Zeta potential of MMSN-2 and MMSN-23 after pDNA binding with 80 μg/mL of MMSN. (b) Gel retardation assay demonstrating pLuc−nanoparticle complexation with increasing amounts of MMSN. The amount of pLuc (4.8 kbp) was constant (0.5 μg). Loading capacity of MMSN-23 is about four times higher than that of MMSN-2. (c) Average amount of loaded plasmids was calculated for both MMSN-2 and MMSN-23. For complexation, 0.5 μg of pDNA was incubated with MMSN in a total volume of 10 μL.

for loading plasmid DNA through electrostatic interaction, the primary amine groups were introduced using 3-aminopropyltriethoxysilane (APTES) through a post-grafting method. The degree of amination on the surface was determined as 3.6 mmol/g for both MMSN-2 (MMSN with 2 nm pore) and MMSN-23 (MMSN with 23 nm pore) by elemental analysis. To facilitate visualization of the MMSN in intracellular delivery, 5-carboxytetramethylrhodamine (TAMRA) dye was conjugated to the particles. The zeta potential of the prepared delivery vehicles after TAMRA conjugation was measured as 12.3 and 17.5 mV for MMSN-2 and MMSN-23, respectively.

Internalization of MMSN into Mammalian Cells. To observe cellular uptake of MMSN-23, TEM and fluorescence microscopy were used for locating the particles. TEM micrograph shows a large number of MMSN were endocytosed by HeLa cells when cells were exposed to 80 μg/mL of MMSN (Figure 2a). The fluorescence micrograph also indicates that TAMRA-labeled MMSN (red fluorescence) were entered into HeLa cells and accumulated around the perinuclear region of the cytoplasm (Figure 2b). Nuclei were stained with DAPI, showing blue fluorescence. These micrographs confirmed that MMSN readily entered into cells across cell membranes without further supplementary materials such as cationic polymers and lipids.

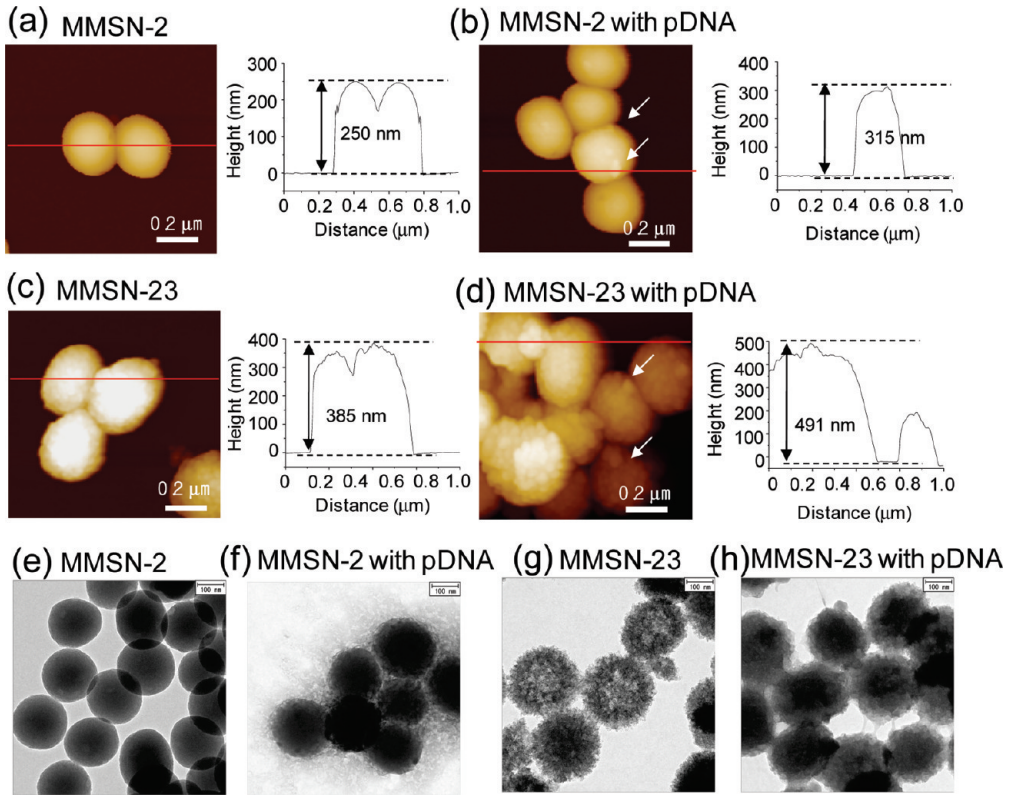

Figure 4. (a, c) AFM and (e, g) TEM images of MMSN-2 and MMSN-23 and (b, d) AFM and (f, h)TEM images of MMSN-2 and MMSN-23 loaded with pLuc. Height profiles indicate that pLuc was loaded onto both MMSN, resulting in increased size of overall nanocomplex. MMSN-23 loaded with pLuc showed rough surface morphology, implying that some portions of the loaded pLuc are extruded from the pores.

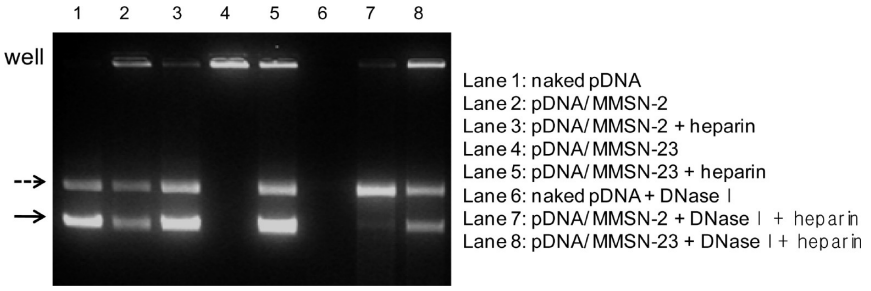

Figure 5. DNase I protection assay. Upper dotted arrow indicates linear form of pDNA, and lower solid arrow indicates supercoiled form of pDNA. The amount of pDNA (0.5 μg) and SiNPs (20 μg) were constant. Lane 1, naked pDNA (pLuc); lane 2, pDNA/MMSN-2; lane 3, pDNA/MMSN-2 after pDNA was released by heparin; lane 4, pDNA/MMSN-23; lane 5, pDNA/MMSN-23 after pDNA was released by heparin; lane 6, naked pDNA treated with DNase I; lane 7, pDNA/MMSN-2 treated with DNase I before pDNA was released by heparin; lane 8, pDNA/MMSN-23 treated with DNase I before pDNA was released by heparin. MMSN-23 showed remarkable protection of pDNA to DNase I degradation.

Loading of Plasmid DNA (pDNA) to MMSN. To evaluate pDNA loading capacity, the surface charge of MMSN was estimated by zeta potential (Figure 3a). As described above, zeta potentials of MMSN-23 and MMSN-2 were 17.5 and 12.3 mV in pH 7.4 buffered solution. After pDNA binding (pLuc, plasmid encoding luciferase, 2 μg/mL) with MMSN (80 μg/mL), the zeta potential of pDNA/MMSN-23 complexes still showed a positive value, 4.53 mV, whereas the pDNA/MMSN-2 complexes gave a highly negative value, −34.5 mV. This result suggests the MMSN-23 has a high loading capacity of pDNA with a high possibility of efficient cellular uptake even after pDNA binding, whereas a MMSN-2 carries pDNA mostly on the outer surface of the particle rather than inside the pores.[31] We next measured hydrodynamic diameters of a pDNA/MMSN complex with a zetasizer after 30 min of co-incubation with pDNA. Hydrodynamic diameters of the particles increased after incubation with pDNA from 905 to 1223 nm and from 543 to 1071 nm for MMSN-2 and MMSN-23, respectively. We observed that longer incubation tends to induce further aggregation over time. This aggregation behavior may attenuate merit of nanosized particles. In addition, it may also lead to

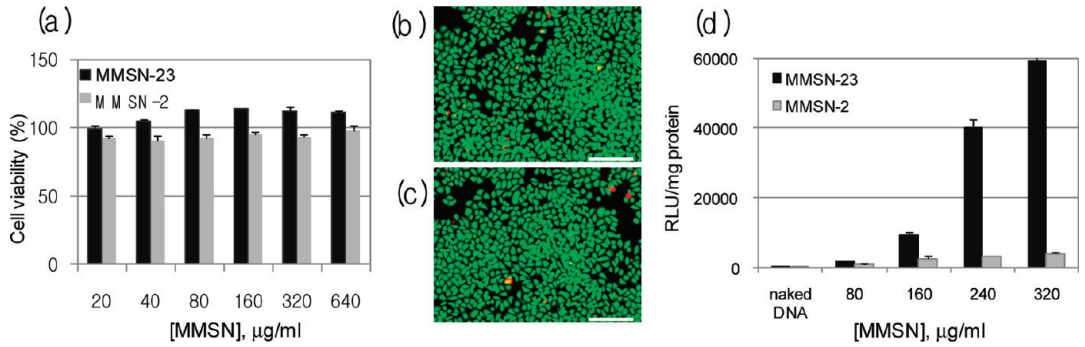

Figure 6. (a) Cell viability of MMSN determined by CCK-8 assay. All samples were run in triplicate. (b, c) Live/dead staining of cells treated with 320 μg/mL of MMSN-23 (b) and untreated (c). Scale bar is 200 μm. (d) *In vitro* transfection efficiency of the luciferase gene (pLuc) into cells with increasing concentration of MMSN-2 and MMSN-23. The amount of pLuc was constant (0.5 μg) and results were normalized to total cell protein.

faster sedimentation in cell culture and thus lead to higher transfection efficiency as compared to nonaggregated particles. To examine loading capacity of pDNA according to the concentration of MMSN, a gel retardation assay was performed with complexes of pDNA and varying concentrations of MMSN-23 and MMSN-2. A constant amount of pDNA (pLuc, 4.8 kbp, 0.5 μg) was complexed with various amounts of MMSN from 5 to 60 μg. MMSN-23 made stable complex with pDNA showing higher amount of condensed pDNA/MMSN-23 complex retained in the well even though smaller amount of MMSN-23 was used than MMSN-2, suggesting that loading capacity of MMSN-23 was higher than MMSN-2 (Figure 3b). The average number of loaded plasmids was calculated based on DNA band intensities on a gel. As expected, MMSN-23 had higher loading capacity for pDNA than MMSN-2 in all the conditions (Figure 3c). The higher plasmid loading capacity of MMSN-23, while maintaining positive zeta potential unlike MMSN-2, suggests that MMSN-23 may have more inner space to hold plasmids than MMSN-2.

Characterization of pDNA/MMSN complex. The pDNA loading to MMSN was further characterized by AFM and TEM. Height profiles of MMSN before (Figure 4a, c) and after (Figure 4b, d) pLuc binding show that pLuc was loaded onto both MMSN, resulting in increased overall size of nanocomplexes. Notably, MMSN-23 loaded with pLuc (Figure 4d) shows many small compact structures on the surface with rough surface morphology, implying higher plasmid loading capacity of MMSN-23 than that of MMSN-2. TEM images also showed changes in morphology of the particles after pDNA loading (Figure 4e, f, g, h). It appears that MMSN-23 shows lower tendency to get aggregated into clusters of nanoparticles than MMSN-2 after pDNA loading (Figure 4h). Both AFM and TEM images suggest that pDNAs are loaded to the MMSN-23 and MMSN-2. One pDNA molecule may adsorb to both inside and outside of the MMSN-23, whereas it may mostly adsorb to the outside of the particles with 2 nm pores.

DNase I Protection Assay. For efficient gene delivery, the pDNA loaded to the gene carrier should be protected against degradation by nucleases.[32] The degree of pDNA degradation under various conditions was examined in the presence of DNase I. After DNase I treatment, the pDNA was released from positively charged carriers by heparin treatment[33] at 50 °C for 60 min right before gel electrophoresis. The loading capacities of pDNA to MMSN-2 and MMSN-23 were different from the beginning (Figure 5, lanes 2,4). In a releasing test without treatment of DNase I (lanes 3, 5), pDNA complexed with MMSN-2 was almost completely released, whereas pDNA with MMSN-23 was not and was retained in the well even with a higher concentration of heparin. This result demonstrated that MMSN-23 formed very stable complexes with pDNA. After DNase I treatment at 37 °C for 30 min, naked pDNA was completely degraded and not detected on the gel (lane 6). The degradation of pDNA proceeded much slower when complexed with MMSN-23 than with MMSN-2 (lane 7, 8) showing that a half of pDNA from pDNA/MMSN-23 after DNase I treatment exists as an intact supercoiled form (lane 8), while pDNA from pDNA/MMSN-2 after DNase I treatment was mostly present as a linear form, not an intact supercoiled form (lane 7). These results suggest that MMSN-23 can more efficiently protect pDNA from nuclease-mediated degradation than MMSN-2.

Cytotoxicity of MMSN-23. For gene therapy, gene carriers would be better to have low cytotoxicity with high biocompatibility. To evaluate toxicity of MMSN-23, HeLa cells were treated with various concentrations of MMSN, and cell viability was determined by CCK-8 assay. Figure 6a shows that the silica nanoparticles did not induce noticeable cell death even at high concentration (640 μg/mL). Live/dead staining shows most cells were viable (green fluorescence) at 320 μg/mL of MMSN-23 with very few dead cells (red fluorescence) (Figure 6b) similar to untreated HeLa cells (Figure 6c).

pLuc (Luciferase Plasmid) and pGFP (GFP Plasmid) Transfection Efficiency. Gene transfection experiments were performed using HeLa cells with MMSN-23 and MMSN-2. The pLuc (0.5 μg) was used as the luciferase reporter

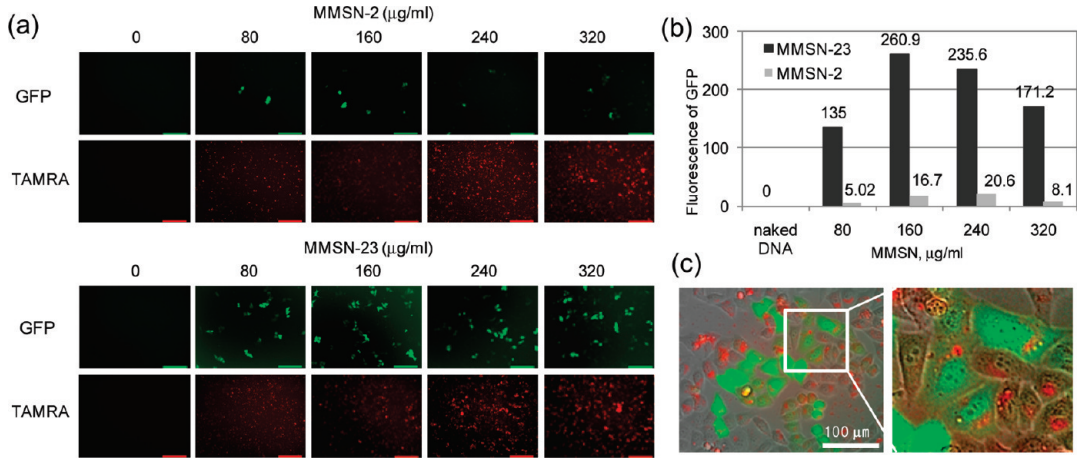

Figure 7. ***In vitro*** **transfection efficiency of the GFP gene (pGFP, 0.5 μg) into HeLa cells. (a) Fluorescence images of GFP expression and TAMRA conjugated to MMSN with increasing concentration of MMSN. Scale bar is 200 μm. (b) Quantification of GFP expression levels by flow cytometry with MMSN-23 and MMSN-2. (c) Fluorescence image showing transfected cells expressed GFP with internalized MMSN-23 (160 μg/mL) with high magnification.**

gene, and the luciferase expression induced by pLuc/MMSN complexes was investigated with increasing amounts of MMSN. Figure 6d shows pLuc/MMSN-2 complexes were not able to induce protein expression inside the cells efficiently even at high concentration. Naked pLuc also showed little or no luciferase expression. However, expression efficiency by pLuc/MMSN-23 complexes increased with increasing amounts of the nanoparticles, as shown in Figure 6d. At a high concentration of MMSN-23 (320 μg/mL), gene expression efficiency was overwhelmingly high compared to MMSN-2 and naked pLuc. These results demonstrate that MMSN-23 not only have a high loading capacity of pDNA, but also can deliver pDNA into cells efficiently.

Gene transfection was also demonstrated using pGFP, a plasmid encoding green fluorescent protein. Figure 7a shows fluorescence images of HeLa cells transfected with pGFP (0.5 μg, 4.7 kbp) loaded to TAMRA-conjugated MMSN-2 and MMSN-23. Cellular uptake was confirmed by TAMRA fluorescence in both particles, but GFP expression was hardly observed with MMSN-2 even at high concentrations. In contrast, pGFP/MMSN-23 showed much higher GFP expression at all concentrations of MMSN-23 with the highest expression at 160 μg/mL of MMSN, calculated from GFP mean fluorescences measured by flow cytometry (Figure 7b). Fluorescence images at high magnification further confirmed the internalization of MMSN-23 and GFP expression (Figure 7c). The result indicates that MMSN-23 could deliver pGFP into the cells efficiently as well as pLuc. In the case of pLuc, transfection efficiency increased as the concentration of MMSN-23 was raised, whereas the highest transfection efficiency was observed at 160 μg/mL of MMSN-23 in pGFP transfection. Since the amount of the two plasmids and the experimental condition were constant, the different trends in gene expression efficiency might be due to differences in kinetics and biological half-lives of pDNA and inequality in toxicity of the expressed proteins.[34] As a control, a pDNA transfection experiment was also performed using lipofectamine 2000 in place of MMSN-23. Lipofectamine 2000 showed higher transfection efficiency than that of MMSN-23 (320 μg/mL) by an average of 3.5-fold. However, lipofectamine 2000 is more cytotoxic than MMSN-23 and induced notable cell death under the experimental condition where same amount of pDNA was applied.[35]

CONCLUSION

We synthesized MMSN with large pores by a facile method and demonstrated that MMSN-23 were an efficient gene delivery carrier compared to MMSN with small pores (~2 nm). MMSN-23 showed efficient cellular uptake, high loading capacity of pDNA, remarkable protection against DNase I, and low cytotoxicity. Most importantly, MMSN-23 enabled efficient gene delivery to deliver plasmids encoding two different proteins, luciferase and GFP, without the assistance of cationic lipids or polymers. Although pDNA is large, transfection and expression of pDNA were successfully accomplished by MMSN-23. To the best of our knowledge, the present study is first to synthesize MMSN with an overall diameter of ~250 nm possessing ultralarge pores of ~23 nm with a simple preparation strategy, which is readily applicable in living systems, and to demonstrate its application as a gene delivery carrier with low cytotoxicity. We believe that MMSN-23 possess high potential as a delivery carrier for other macromolecules such as enzymes and antibodies in addition to plasmids.

MMSN-23 have many advantages such as facile synthesis and modification, large quantity production at competitive cost, and encapsulation of drugs and genes. Among them, it is worth noting that highly aminated MMSN-23 readily enter into cells without any

polymers or lipids in spite of high loading of pDNA. MMSN-23 show efficient cellular uptake only by introduction of amine functionality to the surface. Further, the aminated MMSN-23 would be easily modified to incorporate such functions as cell-specific targeting or chemotherapeutic agents by bioconjugation of functional molecules *via* primary amines on the silica surface. MMSN-23 which have large surface areas may be also harnessed to simultaneously deliver both small drugs and therapeutic biomacromolecules, and therefore induce a synergetic effect. Currently, we are investigating further bioapplications of MMSN-23 for the development of highly sensitive enzyme/small molecule sensors as well as for siRNA and peptide/protein delivery systems *in vitro* and *in vivo*.

METHODS

Materials. Cetyl trimethyl ammonium bromide (CTAB) was purchased from Acros (New Jersey, USA). Ethanol was purchased from Merck (Darmstadt, Germany). 3-Aminopropyltriethoxysilane (APTES), tetramethyl orthosilicate (TMOS), toluene, dimethylsulfoxide (DMSO), and mesitylene (trimethyl benzene, TMB) were purchased from Aldrich Chemical Co. (Milwaukee, WI, USA). Sodium hydroxide was purchased from Junsei Chemical Co. (Tokyo, Japan). All reagents were used as received without further purification. DMEM (Dulbecco's Modified Eagle's Medium), FBS (fetal bovine serum), and PBS (pH 7.4) were purchased from WelGENE Inc. (Daegu, Korea). DNase I was purchased from New England Biolabs Inc. (Ipswich, MA, USA). CCK-8 (Cell Counting Kit-8) and luciferase assay system were purchased from Dojindo Molecular Technologies, Inc. (Rockville, MD, USA) and Promega (Madison, WI, USA), respectively. pLuc encoding luciferase and pGFP encoding green fluorescent protein were used for *in vitro* transfection experiment. Each plasmid was transformed in *Escherichia coli* DH5α and amplified in Luria Broth (Conda, Spain) at 37 °C overnight with shaking at 300 rpm. The plasmids were purified using a QIAGEN Midi plasmid purification kit (QIAGEN, Valencia, CA) according to the manufacturer's protocol. Purified DNA was dissolved in a buffer, and its purity and concentration were measured by NanoDrop 1000 spectrophotometer (Thermo Fischer Scientific, USA).

Synthesis of MMSN-2 and MMSN-23. As-synthesized silica nanoparticles were prepared according to the literature with little modification. In brief, 3.94 mg of CTAB and 2.28 mL of 1 M NaOH solution were dissolved in 800 g of methanol/water (0.4/0.6 = w/w). With vigorous stirring, 1.3 mL of TMOS was added to the solution under ambient condition. After being stirred for 8 h, the mixture was aged overnight. The resulting white precipitate was purified to remove remaining surfactant by centrifugation and washed with ethanol and water five times each. To prepare MMSN-2, as-synthesized silica nanoparticles were suspended in 20 mL of ethanol, and 4 mL of HCl was added to the suspension. The suspension was refluxed overnight. The resulting white powder was filtered out and washed with ethanol. To prepare MMSN-23, as-synthesized silica nanoparticles were dispersed in ethanol by sonication for 30 min, followed by the addition of 20 mL of 1:1 mixture (v/v) of water and TMB. The mixture was placed in the autoclave, and kept at 140 °C for 4 days without stirring. The resulting white powder was washed with ethanol and water five times each. The organic surfactant was removed by refluxing in acidic ethanolic solution as described above for the synthesis of MMSN-2.

Preparation of Amine-Functionalized MMSN-2 and MMSN-23 Conjugated with TAMRA. The prepared MMSN-2 and MMSN-23 (100 mg each) were suspended in toluene followed by the addition of 1 mL of APTES. The suspension was refluxed overnight, filtered out, and washed with ethanol. Amine-grafted MMSN-2 and MMSN-23 (30 mg each) were then suspended in 1 mL of DMSO, and 10 μL of TAMRA NHS solution (2.5 mg/mL in DMSO) was added to the suspension. After stirring for 3 h, the pinkish powder was obtained by centrifugation and washing with ethanol and water five times each.

Characterization of MMSN. Nitrogen adsorption−desorption isotherms were measured at 77 K with 13 and 26 mg of MMSN-2 and MMSN-23, respectively, using a Quantachrome Nova 2000 series analyzer. Before the measurements, all samples were degassed at 300 °C for 12 h. Surface area calculations were carried out using the BET method, whereas the pore size distribution was calculated according to the BJH method.

Cell Culture. HeLa (Human cervical cancer cell line) cells were cultured in DMEM (Dulbecco's Modified Eagle's Medium) containing 4.5 g/L D-glucose and supplemented with 10% FBS (fetal bovine serum), 100 units/mL penicillin, and 100 μg/mL streptomycin. Cells were maintained in a humidified 5% CO_2 incubator at 37 °C.

Transmission Electron Microscopy of MMSN Treated Cells. The MMSN-23 (80 μg/mL) treated cells were fixed with 2.5% glutaraldehyde in PBS for 5 h at 4 °C. The samples were rinsed 3 times in 0.1 M cacodylate buffer and post-fixated with 2% osmium tetroxide (OsO_4) solution for 1 h at 4 °C. Then they were washed and stained with *en bloc* 2% uranyl acetate in distilled water overnight. They were subsequently dehydrated in a graded ethanol series and a Spurr resin (mixture with ERL 4221, DER 736, NSA and DMAE, TedPella Inc.) series. Finally, the samples were placed in fresh 100% Spurr resin in molds and polymerized at 60 °C for 8 h. Ultrathin (50−70 nm) sections were cut with an ultramicrotome (XTXL, RMC) and diamond knife. Then sections were loaded on the copper grids. The grids were stained with 2% uranyl acetate in 50% methanol followed by lead citrate and observed by Tecnai F20 (FEI, Netherlands) at 200 kV.

Cellular uptake of MMSN. HeLa cells were seeded on glass coverslips in a 24-well plate and cultured at 37 °C in an incubator. After 24 h, cells were treated with 80 μg/mL of TAMRA labeled MMSN-23 for 24 h, and then washed with PBS. For fixation, a glass that cells adhered on was immersed in 4% paraformaldehyde in PBS for 10 min at room temperature. Following fixation, the glass was washed with PBS and mounted on a slide with nuclei staining by DAPI. Images were collected using a Ti inverted fluorescence microscope equipped with a 60× (1.4 numerical aperture) objective (Nikon Co., Japan) and a CoolSNAP cf charge-coupled device (CCD) camera (Photometrics, Tucson, AZ).

Zeta Potential Measurement. Zeta potential of MMSN and pDNA/MMSN complexes was measured by Zetasizer Nano ZS (Malvern Instruments, UK). The 80 μg/mL MMSN and MMSN loaded with pLuc (2 μg/mL) were prepared in PBS. After 30 min of incubation with pLuc at 4 °C, data were collected.

Gel Retardation Assay. To prepare each complex, 0.5 μg of pLuc was incubated with varying amounts of MMSN at 4 °C in PBS. After 1 h incubation, loading star (DyneBio Inc., Korea) was added into each mixture, and then mixtures were loaded on a 0.8% agarose gel. The electrophoresis was carried out at 100 V for 30 min in TAE buffer, and the bands were visualized on a UV trans-illuminator.

AFM Measurement. MMSN and pDNA/MMSN complexes prepared by incubation of 0.5 μg pLuc with 20 μg MMSN were suspended in distilled water at 4 °C. After 30 min of incubation, each solution was half diluted with distilled water, and a drop of solution was placed onto the silicon wafer. The wafer was then dried at room temperature for several hours before AFM observation. AFM images and profiles were then taken with a

XE-100 (Park system, Korea) with a backside gold-coated silicon probe (M to N, Korea).

TEM measurement. Transmission electron microscope (TEM) observation was carried out on a Tecnai F20 (Philips, Netherlands) at 200 kV. Samples were prepared in PBS, and a drop of each suspension was placed onto the Formvar-coated copper grid, stabilized with evaporated carbon film (Electron Microscopy Sciences, PA, USA). The grids were then dried at room temperature for several hours before TEM observation.

DNase I Protection Assay. pDNA/MMSN complexes were prepared with 20 μg of MMSN and 0.5 μg of pLuc in 10 μL total volume (in PBS). Naked pLuc (0.5 μg) and complex solutions were incubated with 0.25 U of DNase I (2 units/μL) in 10 mM Tris-HCl, 2.5 mM $MgCl_2$, 0.5 mM $CaCl_2$, pH 7.6, at 37 °C for 30 min. The DNase I was inactivated by adding 1 μL of 500 mM ethylenediaminetetraacetic acid (EDTA). The pLuc was then released from the complex by treatment with heparin (3.4 mg/mL) at 50 °C for 60 min, and analyzed by 0.8% agarose gel electrophoresis.

Cell Viability Test of MMSN. The cytotoxicity of MMSN was tested by examining the viability of HeLa cells after MMSN treatment using CCK-8 assay. HeLa cells were seeded in a 96-well cell culture plate 24 h before MMSN treatment at a density of 1×10^4 cells/well. Following incubation, the cells were added with various concentrations of MMSN, and control cells were added with equivalent volume of PBS. After 24 h, media containing MMSN was removed, and 100 μL of serum-free media and 10 μL of CCK-8 solution were added to each well. Plate was then incubated under cell culture conditions for 1 h. The optical density of formazan salt at 450 nm was measured using a microplate reader (Molecular Devices, Inc., USA), and background absorbance of media was subtracted. Experiment was carried out in triplicate, and data were shown as mean ± SEM.

Live/Dead Staining of MMSN-Treated Cells. The biocompatibility of MMSN-23 was evaluated using the Live/Dead Viability/Cytotoxicity Assay Kit (Molecular Probes Invitrogen). HeLa cells were seeded in a 96-well cell culture plate 24 h before MMSN-23 treatment at a density of 1×10^4 cells/well. The cells were then incubated with 320 μg/mL of MMSN-23, and untreated cells were added with equivalent volume of PBS. After 24 h, media containing MMSN-23 was discarded and cells were washed with PBS. Following washing, 50 μL of the combined live-dead cell staining solution (2 μM Calcein AM and 4 μM EthD-1 in D-PBS) was added to each well and incubated with cells for 20 min at room temperature. Images of live (green fluorescence) and dead (red fluorescence) cells were obtained using a Ti inverted fluorescence microscope.

pLuc (Luciferase Plasmid) Transfection and Luciferase Assay. HeLa cells were seeded in a 24-well cell culture plate at a density of 4×10^4 cells/well 24 h before transfection. Prior to transfection, pLuc/MMSN complexes were freshly prepared as follows: 0.5 μg of pLuc (pGL3) was incubated with various amounts of MMSN, from 0 to 80 μg, in PBS at 4 °C for 1 h. Each mixture (total volume of 10 μL) was then diluted with 240 μL of serum-free media. pLuc/MMSN complexes in serum-free media (250 μL) were added to the cells and incubated at 37 °C. After 4 h, cells were washed with PBS and incubated for additional 48 h in 500 μL of fresh serum-containing media. All transfections were performed in triplicate. Following incubation, cells were washed with PBS and then treated with 100 μL of 1X passive lysis buffer. The cell culture plate was rocked at room temperature for 15 min. Next, the lysate was centrifuged at 14000 rpm for 5 min. Supernatant (20 μL) was added to 60 μL of luciferase assay reagent, and luminescence of samples was measured by a MicroLumat LB 96P bioluminometer (EG&G Berthold, Bad Wildbad, Germany). The relative light units (RLU) were normalized against protein concentration in the cell lysate, measured by a Bradford assay. Luciferase activity was expressed as RLU/mg protein in the cell lysate. Data were shown as mean ± SEM for triplicate samples.

pGFP (GFP plasmid) Transfection and GFP Expression. Condition of cell plating, pGFP/MMSN complex preparation, and complex treatment to cells were the same as in the pLuc transfection experiment. After 48 h of incubation in serum-containing media, GFP expression and TAMRA-labeled MMSN were observed through Ti inverted fluorescence microscope. For quantification, the fluorescence intensity of positive cells was measured with a FACSCalibur flow cytometer (Becton Dickinson, USA) equipped with an argon laser. Transfection efficiency was shown as mean fluorescence of GFP.

Acknowledgment. This work was supported by Basic Science Research Program through the National Research Foundation of Korea (NRF) funded by the Korean government (MEST) (Grant Nos. 313-2008-2-C00538, 2008-0062074), by the Nano R&D program of NRF funded by MEST (2008-2004457), and by the National Honor Scientist Program (20100029665) and World Class University Program (R31-2010-000-10071-0) of NRF funded by MEST. H. Jeon was partially supported by a GRL "Theragnosis" grant from the Korean Government (MEST) and thanks the Advanced Analysis Center in KIST (Korea Institute of Science & Technology) for use of the TEM.

REFERENCES AND NOTES

1. McCormick, F. Cancer Gene Therapy: Fringe or Cutting Edge? *Nat. Rev. Cancer* **2001,** *1*, 130–141.
2. Cross, D.; Burmester, J. K. Gene Therapy for Cancer Treatment: Past, Present and Future. *Clin. Med. Res.* **2006,** *4*, 218–227.
3. Brannon-Peppas, L.; Ghosn, B.; Roy, K.; Cornetta, K. Encapsulation of Nucleic Acids and Opportunities for Cancer Treatment. *Pharm. Res.* **2007,** *24*, 618–627.
4. Kim, S. I.; Shin, D.; Lee, H.; Ahn, B. Y.; Yoon, Y.; Kim, M. Targeted Delivery of siRNA against Hepatitis C Virus by Apolipoprotein A-I-Bound Cationic Liposomes. *J. Hepatol.* **2009,** *50*, 479–488.
5. Yang, X.; Haurigot, V.; Zhou, S.; Luo, G.; Couto, L. B. Inhibition of Hepatitis C Virus Replication Using Adeno-Associated Virus Vector Delivery of an Exogenous Anti-Hepatitis C Virus Microrna Cluster. *Hepatology* **2010,** *52*, 1877–1887.
6. Blouin, M. J.; Beauchemin, H.; Wright, A.; De Paepe, M.; Sorette, M.; Bleau, A. M.; Nakamoto, B.; Ou, C. N.; Stamatoyannopoulos, G.; Trudel, M. Genetic Correction of Sickle Cell Disease: Insights Using Transgenic Mouse Models. *Nat. Med.* **2000,** *6*, 177–182.
7. Pawliuk, R.; Westerman, K. A.; Fabry, M. E.; Payen, E.; Tighe, R.; Bouhassira, E. E.; Acharya, S. A.; Ellis, J.; London, I. M.; Eaves, C. J.; *et al*. Correction of Sickle Cell Disease in Transgenic Mouse Models by Gene Therapy. *Science* **2001,** *294*, 2368–2371.
8. Thomas, C. E.; Ehrhardt, A.; Kay, M. A. Progress and Problems with the Use of Viral Vectors for Gene Therapy. *Nat. Rev. Genet.* **2003,** *4*, 346–358.
9. De Smedt, S. C.; Demeester, J.; Hennink, W. E. Cationic Polymer Based Gene Delivery Systems. *Pharm. Res.* **2000,** *17*, 113–126.
10. Aris, A.; Villaverde, A. Modular Protein Engineering for Non-viral Gene Therapy. *Trends Biotechnol.* **2004,** *22*, 371–377.
11. Panyam, J.; Labhasetwar, V. Biodegradable Nanoparticles for Drug and Gene Delivery to Cells and Tissue. *Adv. Drug Delivery Rev.* **2003,** *55*, 329–347.
12. Zhang, X. Q.; Chen, M.; Lam, R.; Xu, X.; Osawa, E.; Ho, D. Polymer-Functionalized Nanodiamond Platforms as Vehicles for Gene Delivery. *ACS Nano* **2009,** *3*, 2609–2616.
13. Lv, H.; Zhang, S.; Wang, B.; Cui, S.; Yan, J. Toxicity of Cationic Lipids and Cationic Polymers in Gene Delivery. *J. Controlled Release* **2006,** *114*, 100–109.
14. Xu, Z. P.; Hua Zeng, Q.; Lu, G. Q.; Bing, Yu, A. Inorganic Nanoparticles as Carriers for Efficient Cellular Delivery. *Chem. Eng. Sci.* **2006,** *61*, 1027–1040.
15. Rhim, W. K.; Kim, J. S.; Nam, J. M. Lipid−Gold-Nanoparticle Hybrid-Based Gene Delivery. *Small* **2008,** *4*, 1651–1655.
16. Ghosh, P. S.; Kim, C. K.; Han, G.; Forbes, N. S.; Rotello, V. M. Efficient Gene Delivery Vectors by Tuning the Surface Charge Density of Amino Acid-Functionalized Gold Nanoparticles. *ACS Nano* **2008,** *2*, 2213–2218.

17. Derfus, A. M.; Chen, A. A.; Min, D.-H.; Ruoslahti, E.; Bhatia, S. N. Targeted Quantum Dot Conjugates for siRNA Delivery. *Bioconjugate Chem.* **2007,** *18*, 1391–1396.
18. Li, D.; Li, G.; Guo, W.; Li, P.; Wang, E.; Wang, J. Glutathione-Mediated Release of Functional Plasmid DNA from Positively Charged Quantum Dots. *Biomaterials* **2008,** *29*, 2776–2782.
19. Fu, H.; Hu, Y.; McNelis, T.; Hollinger, J. O. A Calcium Phosphate-Based Gene Delivery System. *J. Biomed. Mater. Res. A* **2005,** *74*, 40–48.
20. Pantarotto, D.; Singh, R.; McCarthy, D.; Erhardt, M.; Briand, J. P.; Prato, M.; Kostarelos, K.; Bianco, A. Functionalized Carbon Nanotubes for Plasmid DNA Gene Delivery. *Angew. Chem., Int. Ed.* **2004,** *43*, 5242–5246.
21. Gao, L.; Nie, L.; Wang, T.; Qin, Y.; Guo, Z.; Yang, D.; Yan, X. Carbon Nanotube Delivery of the GFP Gene into Mammalian Cells. *ChemBioChem* **2006,** *7*, 239–242.
22. Hom, C.; Lu, J.; Tamanoi, F. Silica Nanoparticles as a Delivery System for Nucleic Acid-Based Reagents. *J. Mater. Chem.* **2009,** *19*, 6308–6316.
23. Xia, T.; Kovochich, M.; Liong, M.; Meng, H.; Kabehie, S.; George, S.; Zink, J. I.; Nel, A. E. Polyethyleneimine Coating Enhances the Cellular Uptake of Mesoporous Silica Nanoparticles and Allows Safe Delivery of siRNA and DNA Constructs. *ACS Nano* **2009,** *3*, 3273–3286.
24. Radu, D. R.; Lai, C. Y.; Jeftinija, K.; Rowe, E. W.; Jeftinija, S.; Lin, V. S. A Polyamidoamine Dendrimer-Capped Mesoporous Silica Nanosphere-Based Gene Transfection Reagent. *J. Am. Chem. Soc.* **2004,** *126*, 13216–13217.
25. Liu, J.; Stace-Naughton, A.; Brinker, C. J. Silica Nanoparticle Supported Lipid Bilayers for Gene Delivery. *Chem. Commun.* **2009,** *14*, 5100–5102.
26. Lewis, R. J.; Huang, J. H.; Pecora, R. Rotational and Translational Motion of Supercoiled Plasmids in Solution. *Macromolecules* **1985,** *18*, 944–948.
27. Tam, P.; Monck, M.; Lee, D.; Ludkovski, O.; Leng, E. C.; Clow, K.; Stark, H.; Scherrer, P.; Graham, R. W.; Cullis, P. R. Stabilized Plasmid-Lipid Particles for Systemic Gene Therapy. *Gene Ther.* **2000,** *7*, 1867–1874.
28. Kienberger, F.; Costa, L. T.; Zhu, R.; Kada, G.; Reithmayer, M.; Chtcheglova, L.; Rankl, C.; Pacheco, A. B.; Thalhammer, S.; Pastushenko, V.; *et al.* Dynamic Force Microscopy Imaging of Plasmid DNA and Viral RNA. *Biomaterials* **2007,** *28*, 2403–2411.
29. Mizutani, M.; Yamada, Y.; Nakamura, T.; Yano, K. Anomalous Pore Expansion of Highly Monodispersed Mesoporous Silica Spheres and Its Application to the Synthesis of Porous Ferromagnetic Composite. *Chem. Mater.* **2008,** *20*, 4777–4782.
30. Yano, K.; Fukushima, Y. Synthesis of Mono-dispersed Mesoporous Silica Spheres with Highly Ordered Hexagonal Regularity Using Conventional Alkyltrimethylammonium Halide as a Surfactant. *J. Mater. Chem.* **2004,** *14*, 1579–1584.
31. For a previous report on adsorption of linear DNA to mesoporous silica nanoparticles, see: Solberg, S. M.; Landry, C. C. Adsorption of DNA into Mesoporous Silica. *J. Phys. Chem. B* **2006,** *110*, 15261–15268.
32. Escriou, V.; Ciolina, C.; Lacroix, F.; Byk, G.; Scherman, D.; Wils, P. Cationic Lipid-Mediated Gene Transfer: Effect of Serum on Cellular Uptake and Intracellular Fate of Lipopolyamine/DNA Complexes. *Biochim. Biophys. Acta* **1998,** *1368*, 276–288.
33. Hom, C.; Lu, J.; Liong, M.; Luo, H.; Li, Z.; Zink, J. I.; Tamanoi, F. Mesoporous Silica Nanoparticles Facilitate Delivery of siRNA to Shutdown Signaling Pathways in Mammalian Cells. *Small* **2010,** *6*, 1185–1190.
34. Liu, H.-S.; Jan, M.-S.; Chou, C.-K.; Chen, P.-H.; Ke, N.-J. Is Green Fluorescent Protein Toxic to the Living Cells? *Biochem. Biophys. Res. Commun.* **1999,** *260*, 712–717.
35. Gene expression of the cells treated with pDNA-MMSN23 complex in the presence of serum was negligible even though the MMSN-23 is expected to protect pDNA from serum induced degradation. The reason is not clear at this point.